Supplemental Information

Complexes of MN_2S_2•$Fe(\eta^5$-$C_5R_5)(CO)$ as Platform for Exploring Cooperative Heterobimetallic Effects in HER Electrocatalysis

Pokhraj Ghosh,[#] Manuel Quiroz,[#] Ning Wang,[#,‡] Nattamai Bhuvanesh,[#] Marcetta Y. Darensbourg*,[#]

[#]*Department of Chemistry, Texas A & M University, College Station, Texas 77843, United States*

marcetta@chem.tamu.edu

Electrochemistry

Determination of Overpotential

Calculation of Turnover Frequency (TOF)

Experimental setup for bulk electrolysis and gas chromatography

Gas Chromatograms

Scan Rates

Infrared Spectrum

Positive-ion ESI Mass Spectrum

NMR Spectrum

Crystal Structures

Electrochemistry:

(i) **Determination of Overpotential:**

The overpotential for the complexes **Ni-Fe*'**, **Co-Fe*'** and **Co-Fe'** were determined by the method determined by Appel and Helm.[1] Overpotential is defined as the difference between the thermodynamic potential (E_{H+}) and the catalytic half wave potential ($E_{cat/2}$). The value of E_{H+} is +0.65 V (vs $Fc^{0/+}$ = 0.0 V) in 100 mM trifluoroacetic acid (TFA) in CH_3CN solvent. The potential where the catalytic current (i_{cat}) corresponds to half of its value is defined as the catalytic half wave potential ($E_{cat/2}$). A representative example for the **CoFe*'** complex is shown in Figure S1.

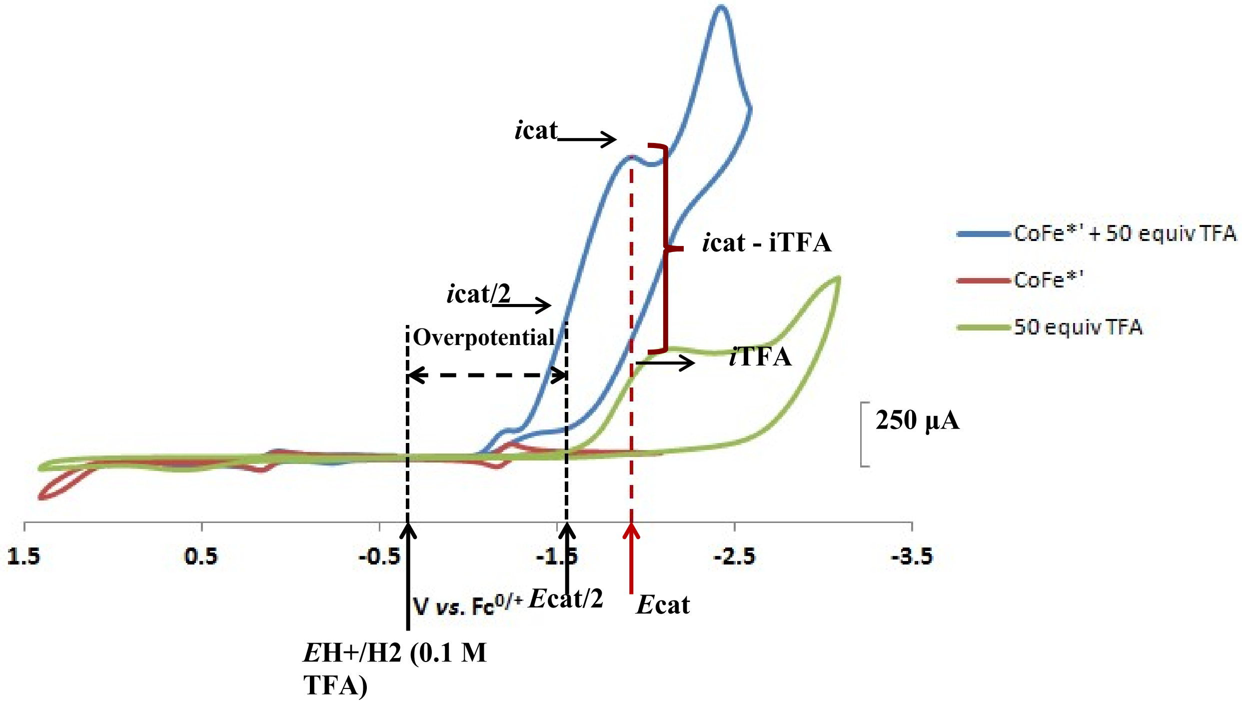

Figure S1. Overalay of cyclic voltammograms of **Co-Fe*'** (red trace), **Co-Fe*'** with 50 equivalents of TFA (blue trace) and 50 equivalents of TFA without catalyst (olive trace). Graphical representation for the calculation of $E_{cat/2}$, net catalytic current (i_{cat}-i_{TFA}) and overpotential is also illustrated.

(ii) **Calculation of Turnover Frequency (TOF):**

TOF frequency was calculated according to the modified equation as published by the Darensbourg group.[2,3] The general form of the equation that uses i_{cat} (Eq. 1) was modified to compensate for the background acid contribution by subtracting the i_{TFA} (Eq 2). The pictorial representation for the corrected catalytic contribution is shown in Figure S1.

$$\mathrm{TOF} = 1.94\ (V^{-1}) \times v\ (Vs^{-1}) \times [i_{cat}/i_p]^2 \qquad \text{(Eq. 1)}$$

TOF = 1.94 (V^{-1}) x v (Vs^{-1}) x $[(i_{cat}-i_{TFA})/i_p]^2$ (Eq. 2)

v = scan rate
i_{cat} = total current measured upon adding acid (TFA) to the catalyst
i_{TFA} = background current measured from the acid (TFA) at the potential of i_{cat}
i_p = current measured from the catalyst in absence of acid
$i_{cat}-i_{TFA}$ = corrected current response from the catalyst only.

The concentration of the acid was sequentially increased until the TOF was fairly constant as shown in Tables S1, S2 and S3 for the complexes **Ni-Fe*'**, **Co-Fe*'** and **Co-Fe'**, respectively.

Table S1. TOF calculation of **Ni-Fe*'** at various concentrations of TFA at scan rate of 0.2 V/s in CH_3CN. The value of i_p was considered at the appearance of the catalytic event at -1.91 V as the first reduction event.

Acid (µL)	**i_{cat} (mA)**	**i_{TFA} (mA)**	**$i_{cat}-i_{TFA}$ (mA)**	**TOF (s^{-1})**
0	0.072	0.000	0.072	0.000
50	0.991	0.664	0.326	7.99
100	1.849	1.247	0.602	27.12
150	2.288	1.677	0.611	27.94
200	2.600	1.943	0.657	32.31

Table S2. TOF calculation of **Co-Fe*'** at various concentrations of TFA at scan rate of 0.2 V/s in CH_3CN. The value of i_p was considered at the appearance of the catalytic event at -1.19 V as the first reduction event.

Acid (µL)	**i_{cat} (mA)**	**i_{TFA} (mA)**	**$i_{cat}-i_{TFA}$ (mA)**	**TOF (s^{-1})**
0	0.053	0.000	0.053	0.000
50	1.184	0.665	0.518	36.56
100	1.907	1.218	0.689	64.69
150	2.299	1.608	0.691	65.06

Table S3. TOF calculation of **Co-Fe'** at various concentrations of TFA at scan rate of 0.2 V/s in CH3CN. The value of i_p was considered at the appearance of the catalytic event at -1.12 V as the first reduction event.

Acid (µL)	**i_{cat} (mA)**	**i_{TFA} (mA)**	**i_{cat}-i_{TFA} (mA)**	**TOF (s^{-1})**
0	0.056	0.000	0.056	0.00
50	1.007	0.454	0.553	37.91
100	1.539	0.848	0.690	59.23
150	1.897	1.125	0.772	74.08
200	2.105	1.307	0.076	79.15

(iii) **Experimental setup for bulk electrolysis and gas chromatography**:

Custom made three-neck truncated conical shaped flaks with an outlet port/gas inlet was the apparatus used for bulk electrolysis experiments. A Ni-Cr-coiled wire counter electrode, a Ag/$AgNO_3$ reference electrode, and a 3 mm glassy carbon working electrode were placed in the necks of the cell. The Ni-Cr-coiled wire placed in a glass tube with a medium glass frit served as the counter electrode. A glass tube containing a Ag wire immersed in a 1 mM solutions of $AgNO_3$ in CH_3CN separated from the main solution by a Vycor frit was the contents of the reference electrode. To the electrochemical cell 10 ml of 0.1 M [n-Bu_4N][PF_6] in MeCN was added and then purged with Ar to remove all O_2. To the cell 2x10^{-5} mol of the appropriate catalyst and 50 equivalents of trifluoroacetic acid were added. To ensure that the experiment was under catalytic conditions, a cyclic voltammogram was recorded. After 30 minutes of bulk electrolysis performed at -1.80 V vs Fc/Fc^+, 1 mL of methane was added as the internal standard.

An Agilent Trace 1300 GC attached with a thermal conductivity detector and a custom-made 120 cm stainless steel coloumn packed with Carbosieve-II was used to identify gases. The column was kept at a temperature of 200 °C and Ar was used to carry the gas during the separation. The detector was set to a temperature of 250 °C. Approximately 200 µL are withdrawn from the headspace gas after bulk electrolysis to quantify H_2 production. The syringe used was a 0.5 mL Valco Precision Sampling Syringe (Series A-2) equipped with a Valco Precision sampling needle with a 5 point side port. By determining the relative response factor of H_2 and the internal standard, H_2 can be quantified. A calibration curve was used that plotted $\frac{are\ of\ H_2}{area\ of\ CH_4} vs \frac{mL\ of\ H_2}{mL\ of\ CH_4}$. It was calculated previously in our lab by recording the gas chromatograms of different amounts of H_2 vs 1 mL of methane. The calibration curve had the linear equation of y = 2.9757x + 0.0226 with R^2 value of 0.9987.[3]

Three bulk electrolysis experiments at -1.80 V in CH_3CN were carried out with 100 mmol of TFA, in absence of catalyst. The average charge passed and faradic efficiency over three experiments was 2.16 ±

0.03 C and 95.58% ± 0.91% respectively. The charge passed vs time plots and gas chromatograms are shown in Figures S2 and S6-S8 and the results are tabulated in Table S4. The background H_2 produced from TFA was accounted for by subtracting the former from the total H_2 produced from the bulk electrolysis experiments with 2 mM catalyst and 50 equivalents of TFA. The gas chromatograms from the bulk electrolysis experiments with the catalysts are shown in Figure S9-S14. We posit that the peak at ca. 2.3 min in the gas chromatograms is due to N_2/O_2 from the atmosphere that contaminated the needle of the gas-tight syringe prior to the insertion of the head space gas into the gas chromatograph. The faradic efficiency and the corrected TON are tabulated in tables S5-S7.

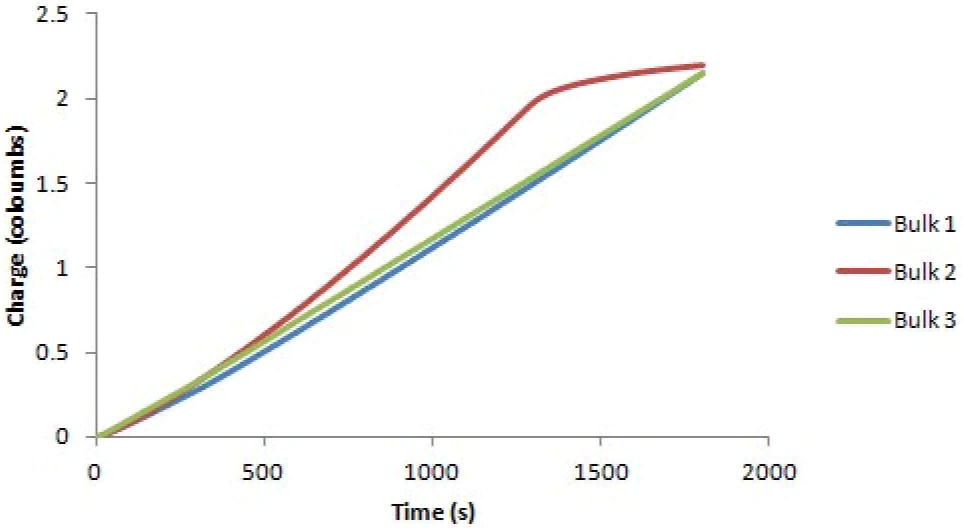

Figure S2. Charge passed (in coulombs) in 30 minutes for the bulk electrolysis of 100 mmol TFA (free acid) in CH_3CN at -1.80 V.

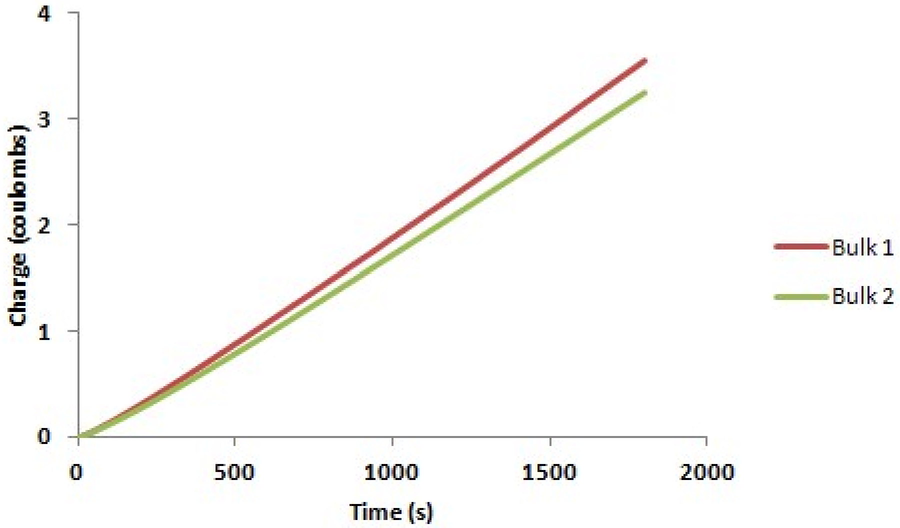

Figure S3. Charge passed (in coulombs) in 30 minutes for the bulk electrolysis of **Ni-Fe*'** in presence of 50 equivalents of TFA in CH_3CN at -1.80 V.

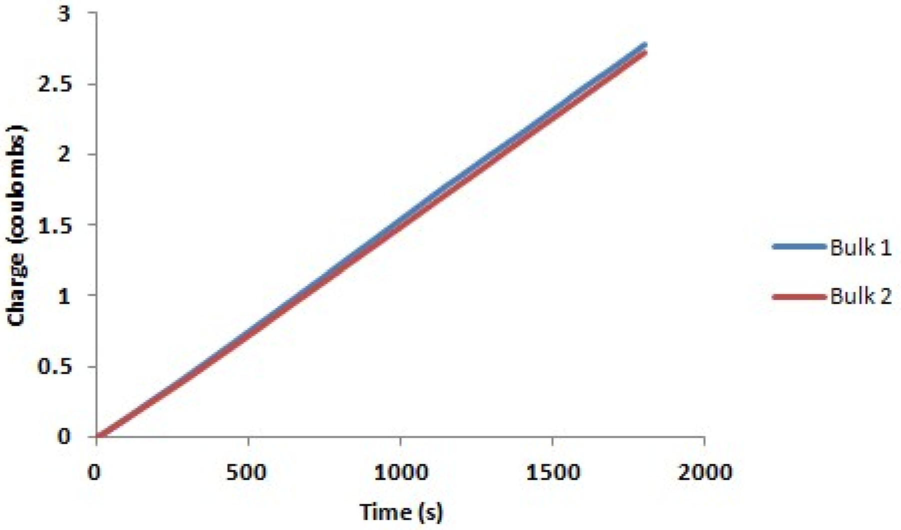

Figure S4. Charge passed (in coulombs) in 30 minutes for the bulk electrolysis of **Co-Fe*'** in presence of 50 equivalents of TFA in CH_3CN at -1.80 V.

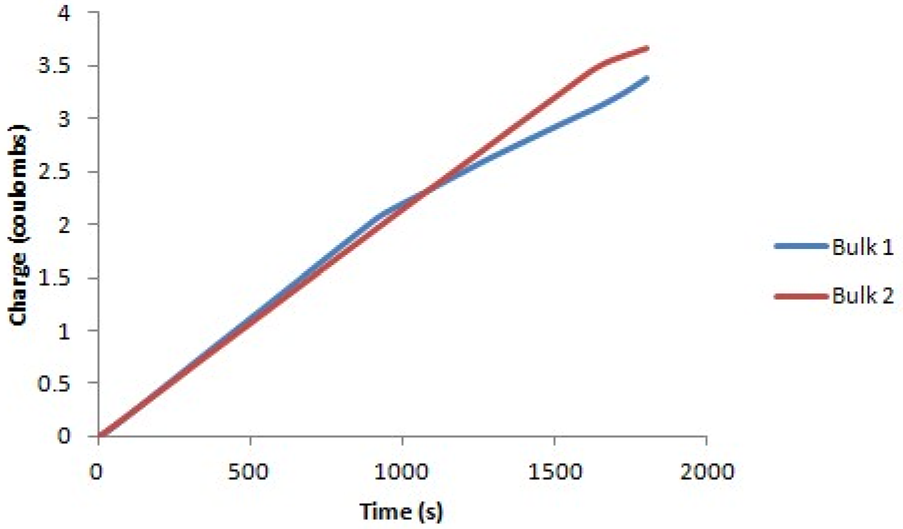

Figure S5. Charge passed (in coulombs) in 30 minutes for the bulk electrolysis of **Co-Fe'** in presence of 50 equivalents of TFA in CH_3CN at -1.80 V.

Table S4. Charge passed (C) and Faradaic efficiency from bulk electrolysis experiments of 100 mM TFA in CH_3CN at -1.80 V for 30 min.

Exp.	Coulombs passed (C)	Area of H_2	Area of CH_4	Ratio: $Area_{H2}/Area_{CH4}$	Theoretical H_2 (mL)	Observed H_2 (mL)	Faradaic Efficiency (%)
1	2.147	0.251	0.318	0.789	0.273	0.257	94.55
2	2.197	0.253	0.308	0.822	0.279	0.269	96.29
3	2.151	0.237	0.296	0.802	0.273	0.262	95.88

Average Coulombs passed = 2.165 ± 0.03
Theoretical H_2 (mL) = (((Coulombs passed/96500)/2)*24.5)*1000
Observed H_2 (mL) = (Ratio-0.0226)/2.9757
Faradaic Efficiency = [Observed H_2/Theoretical H_2]*100

Table S5. Charge passed (C) and corrected TON from bulk electrolysis experiments of 2mM **Ni-Fe*’** and 50 equivalents of TFA in CH_3CN at -1.80 V for 30 min.

Experiment	Charge Passed (C)	Corrected Charge Passed (C)	Faradaic Efficency (%)	TON	Corrected TON
1	3.55	1.38	85.40	0.91	0.35
2	3.26	1.09	91.06	0.85	0.29
Average	3.40 ± 0.20	1.24 ± 0.20	88.23 ± 4.00	0.88 ±0.05	0.32 ± 0.05

Faradaic Efficiency was calculated in the same way as that of the free acid TFA.
TON = (Coulombs passed/(Amount of cat (in mmol)*(0.00001)*96500*2)
Corrected Coulombs (C) = Coulombs passed - Average Coulombs passed for TFA only

Corrected TON = (Corrected Coulombs passed/(Amount of cat (in mmol)*(0.00001)*96500*2)

Table S6. Charge passed (C) and corrected TON from bulk electrolysis experiments of 2mM **Co-Fe*'** and 50 equivalents of TFA in CH_3CN at -1.80 V for 30 min.

Experiment	Charge passed (C)	Corrected Charge passed (C)	Faradaic Efficency (%)	TON	Corrected TON
1	2.78	0.62	99.38	0.72	0.16
2	2.72	0.56	99.15	0.70	0.14
Average	2.75 ± 0.04	0.59 ± 0.04	99.27 ± 0.16	0.71 ± 0.01	0.15 ± 0.01

Table S7. Charge passed (C) and corrected TON from bulk electrolysis experiments of 2mM **Co-Fe'** and 50 equivalents of TFA in CH_3CN at -1.80 V for 30 min.

Experiment	Charge passed (C)	Corrected Charge passed (C)	Faradaic Efficency (%)	TON	Corrected TON
1	3.66	1.49	93.55	0.95	0.32
2	3.38	1.22	92.00	0.88	0.38
Average	3.52 ± 0.20	1.36 ± 0.20	92.76 ± 1.10	0.91 ± 0.05	0.35 ± 0.05

Gas Chromatograms:

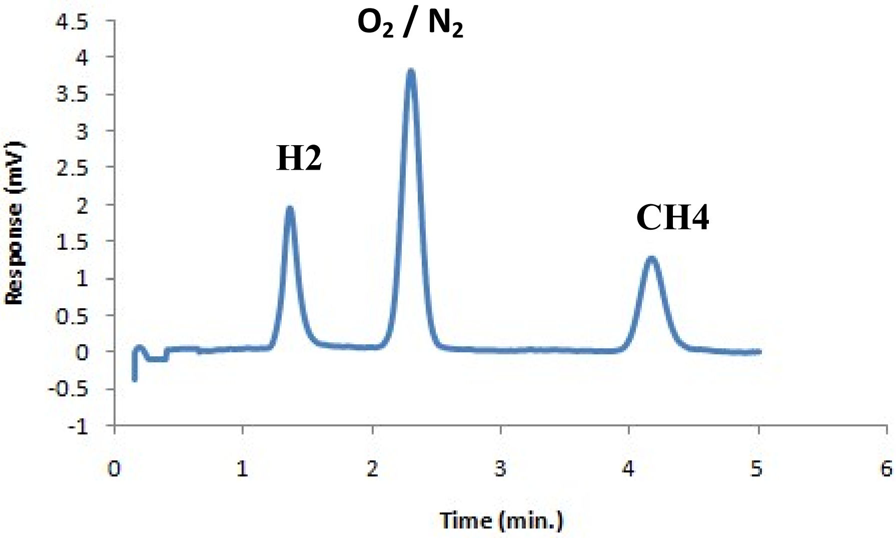

Figure S6. Gas chromatogram from bulk electrolysis experiment 1 at -1.80 V with 100 mmol of TFA (free acid) for 30 min in CH_3CN.

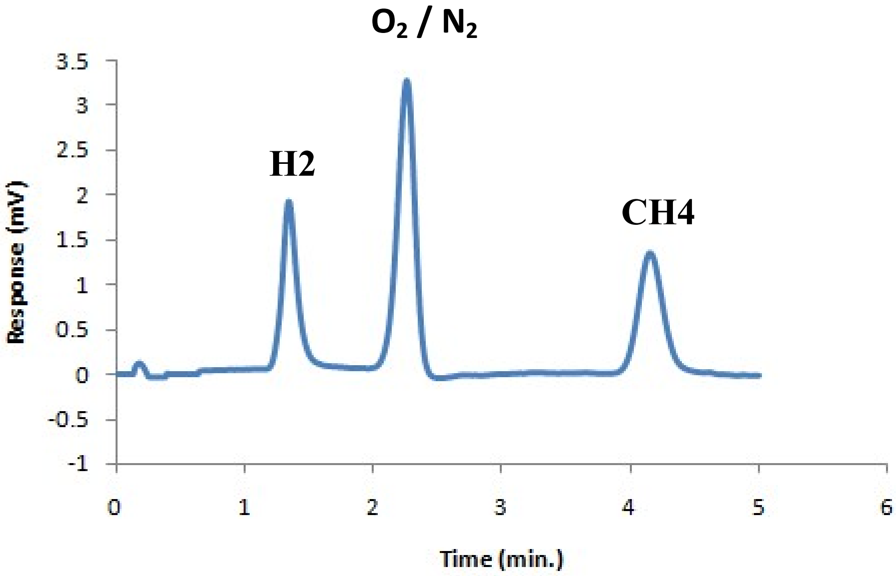

Figure S7. Gas chromatogram from bulk electrolysis experiment 2 at -1.80 V with 100 mmol of TFA (free acid) for 30 min in CH_3CN.

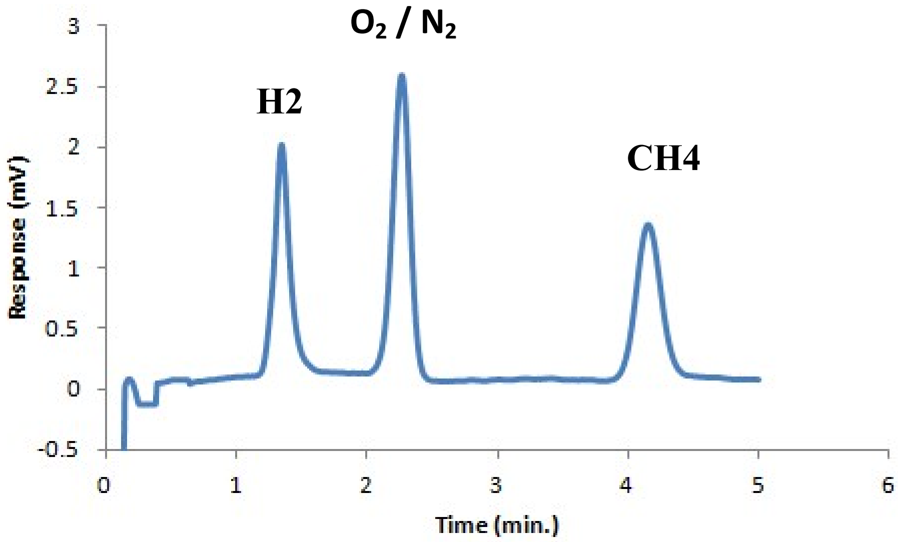

Figure S8. Gas chromatogram from bulk electrolysis experiment 3 at -1.80 V with 100 mmol of TFA (free acid) for 30 min in CH_3CN.

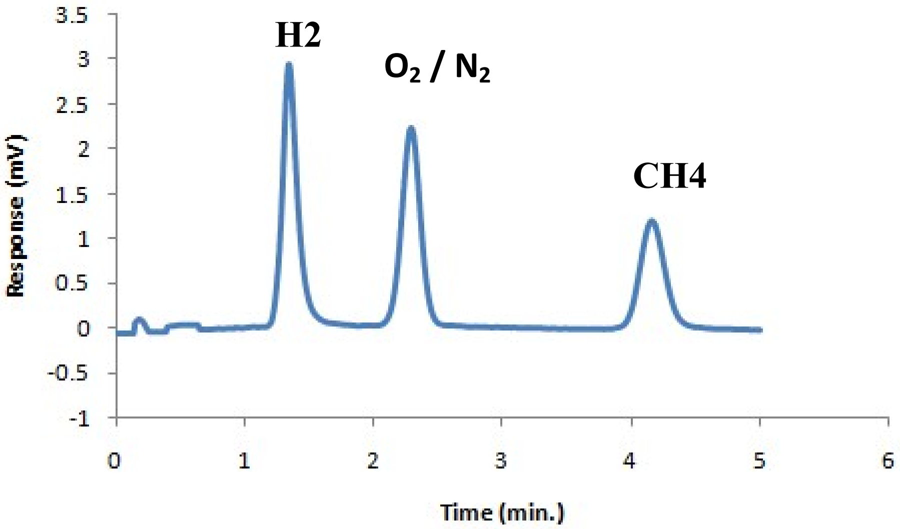

Figure S9. Gas chromatogram from bulk electrolysis experiment 1 at -1.80 V with 2mM **Ni-Fe*'** and 50 equivalents of TFA for 30 min in CH_3CN.

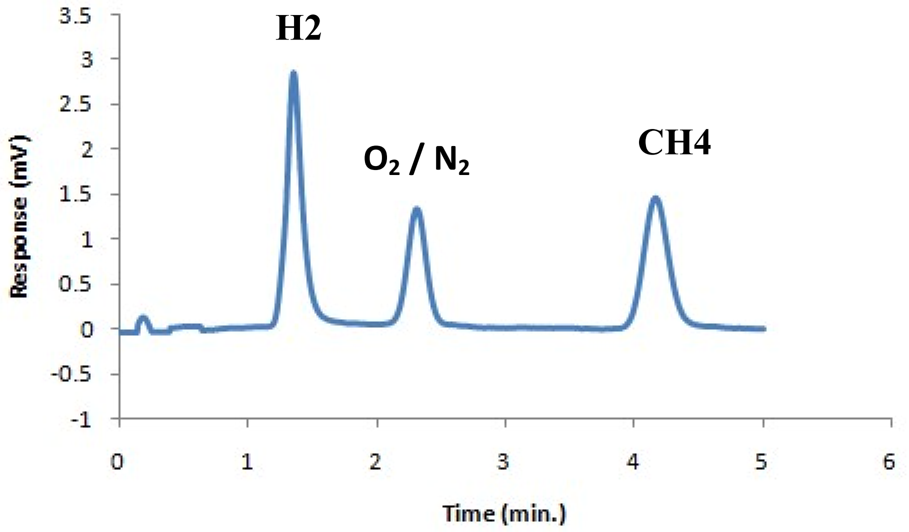

Figure S10. Gas chromatogram from bulk electrolysis experiment 2 at -1.80 V with 2mM **Ni-Fe*'** and 50 equivalents of TFA for 30 min in CH_3CN.

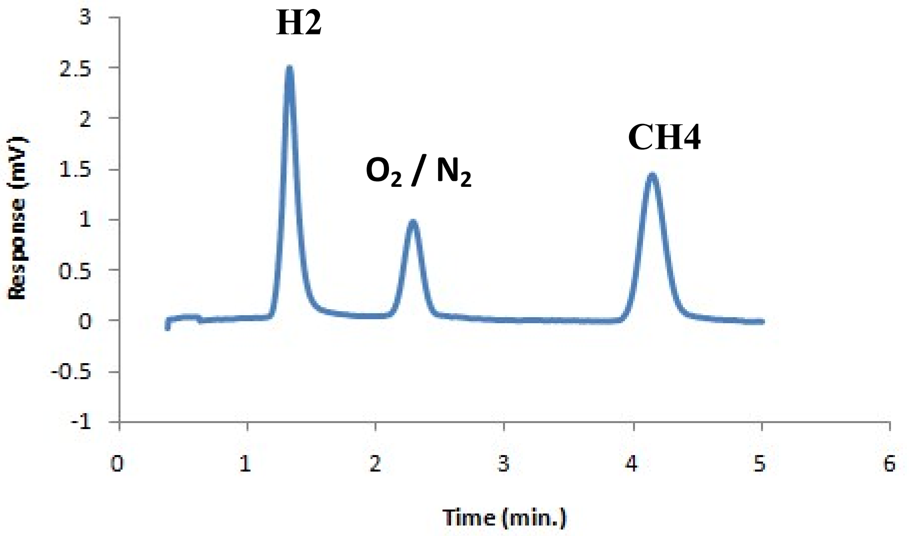

Figure S11. Gas chromatogram from bulk electrolysis experiment 1 at -1.80 V with 2mM **Co-Fe*'** and 50 equivalents of TFA for 30 min in CH_3CN.

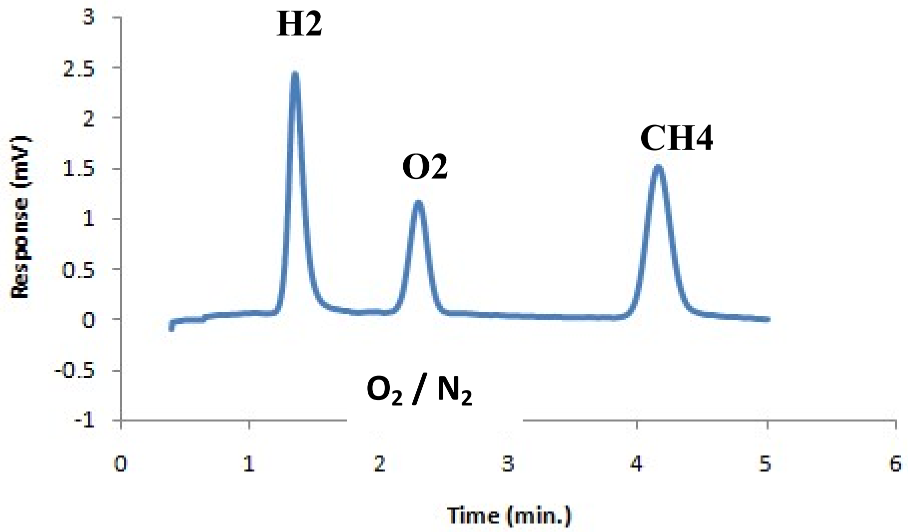

Figure S12. Gas chromatogram from bulk electrolysis experiment 2 at -1.80 V with 2mM **Co-Fe*'** and 50 equivalents of TFA for 30 min in CH_3CN.

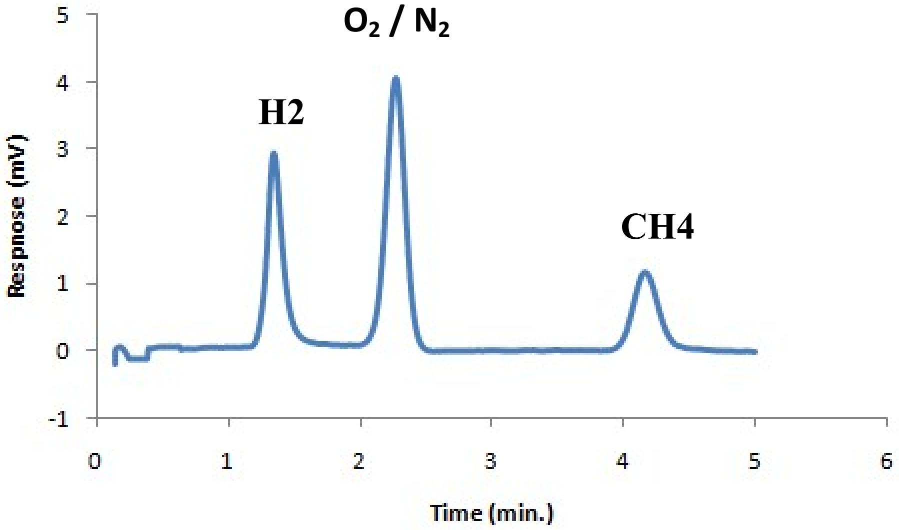

Figure S13. Gas chromatogram from bulk electrolysis experiment 1 at -1.80 V with 2mM **Co-Fe'** and 50 equivalents of TFA for 30 min in CH_3CN.

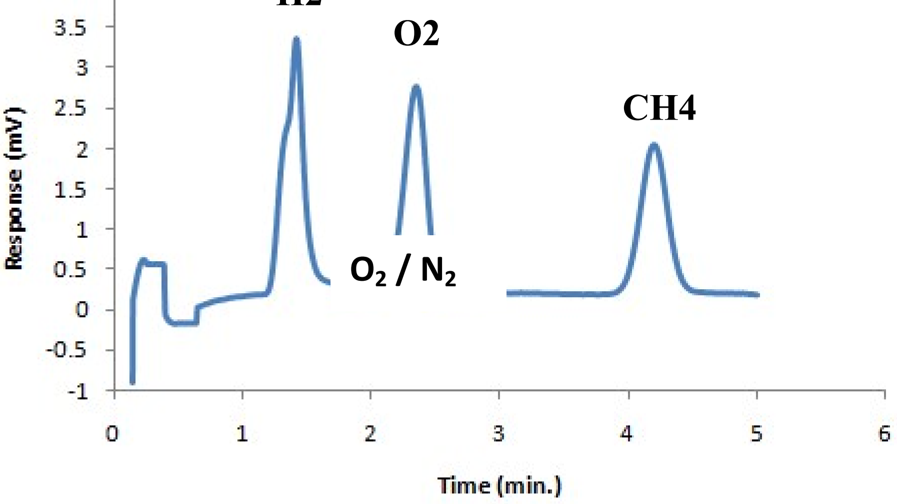

Figure S14. Gas chromatogram from bulk electrolysis experiment 2 at -1.80 V with 2mM **Co-Fe’** and 50 equivalents of TFA for 30 min in CH_3CN.

Scan Rates:

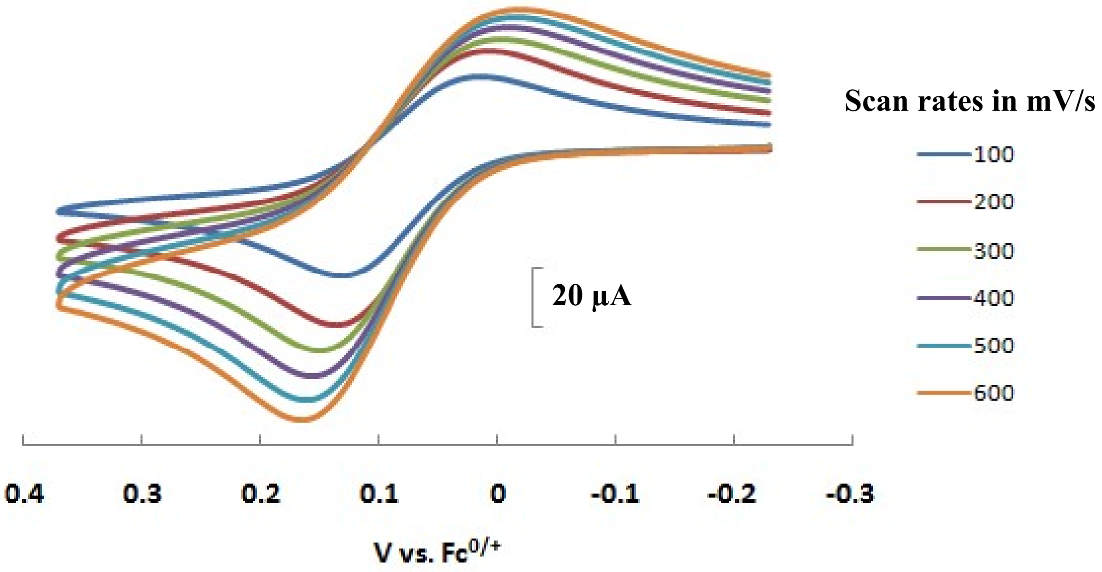

Figure S15. The oxidation event, Cp*Fe’$^{II/III}$ ($E_{1/2}$ = 0.07 V), of **Ni-Fe*’**, recorded at different scan rates in CH_3CN referenced to Fc$^{0/+}$.

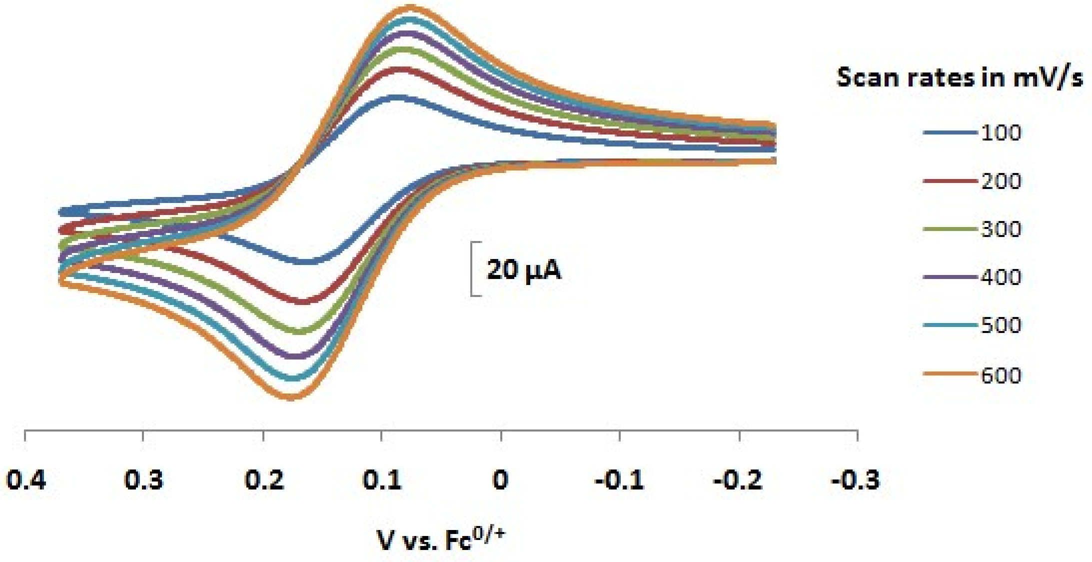

Figure S16. The oxidation event, Cp*Fe'$^{II/III}$ ($E_{1/2}$ = 0.12 V), of **Co-Fe*'**, recorded at different scan rates in CH_3CN referenced to Fc$^{0/+}$.

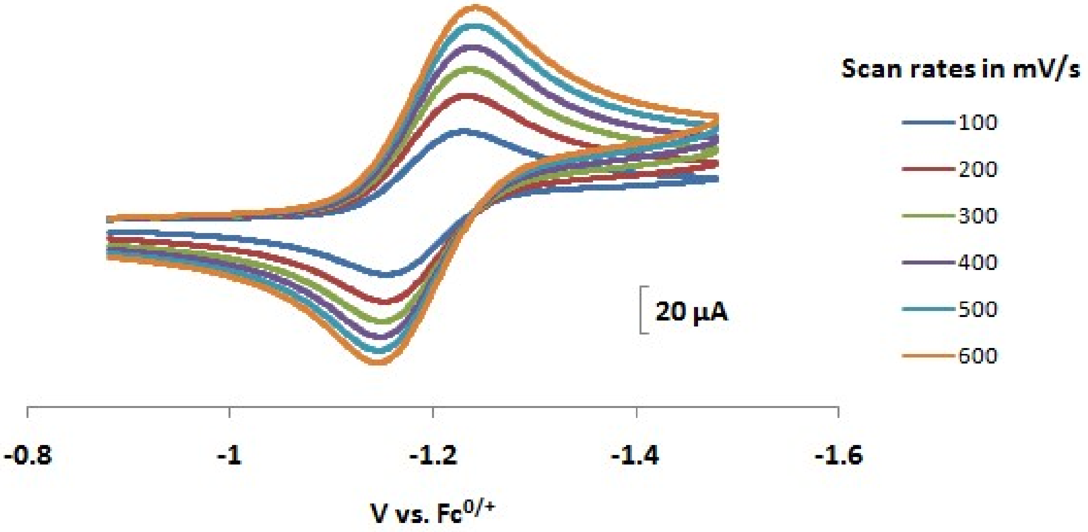

Figure S17. The reduction event, {Co(NO)}$^{8/9}$ ($E_{1/2}$ = -1.19 V), of **Co-Fe*'**, recorded at different scan rates in CH_3CN referenced to Fc$^{0/+}$.

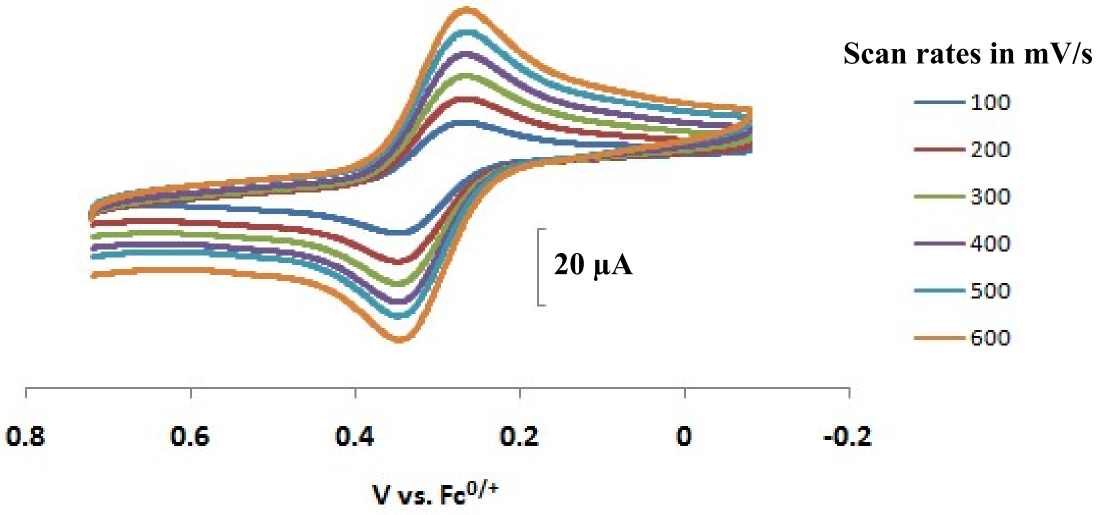

Figure S18. The oxidation event, CpFe'$^{\mathrm{II/III}}$ ($E_{1/2}$ = 0.32 V), of **Co-Fe'**, recorded at different scan rates in CH_3CN referenced to Fc$^{0/+}$.

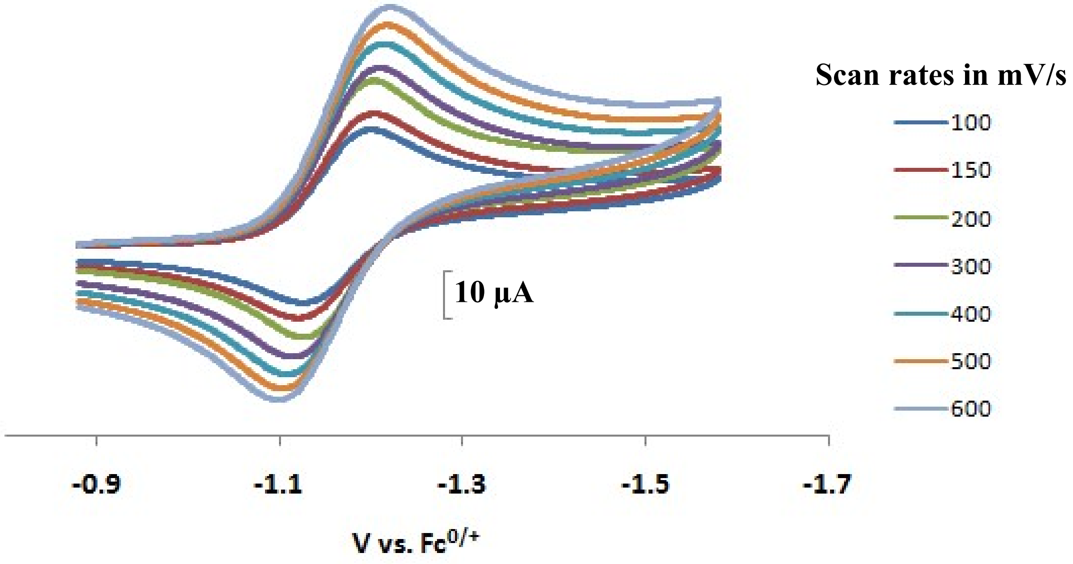

Figure S19. The reduction event, {Co(NO)}$^{8/9}$ ($E_{1/2}$ = -1.12 V), of **Co-Fe'**, recorded at different scan rates in CH_3CN referenced to Fc$^{0/+}$.

IR Spectrum:

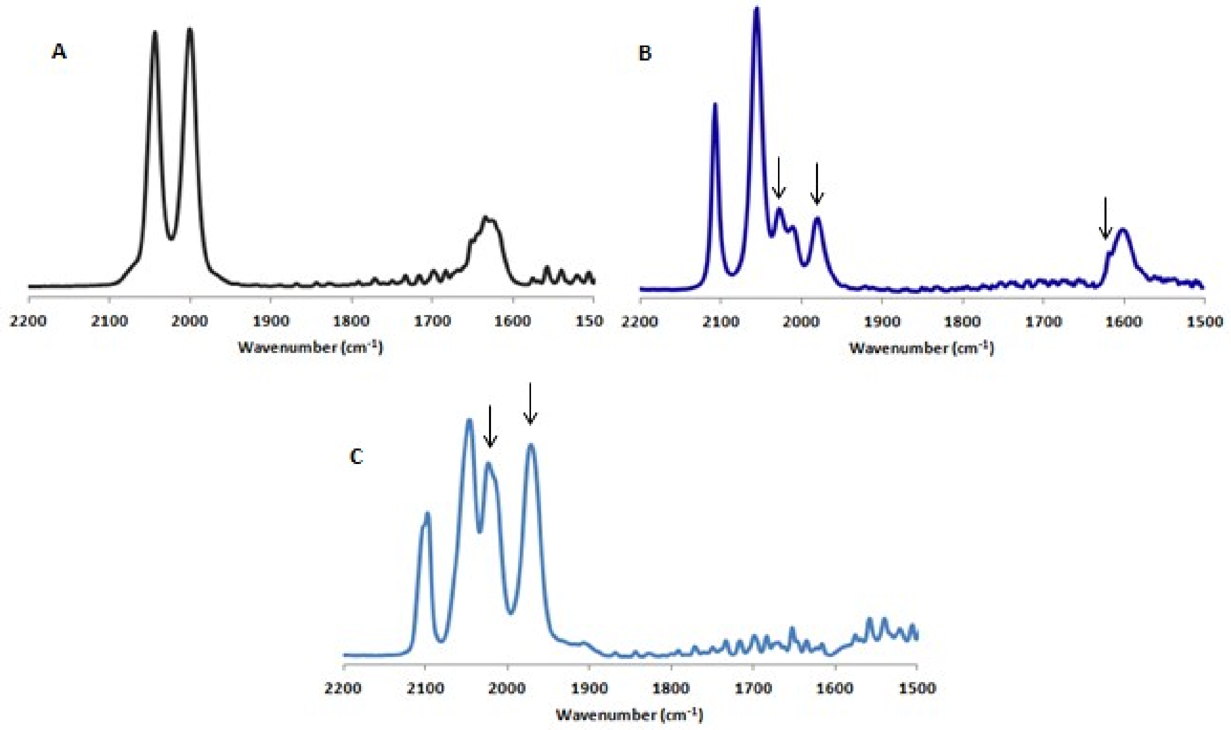

Figure S20. IR spectrum of (A) **Co-Fe”**, (B) **Co-Fe*”**, (C) **Ni-Fe*”** in CH_2Cl_2. Note for **Co-Fe*”** and **Ni-Fe*”** the peaks of the product are shown by arrow.

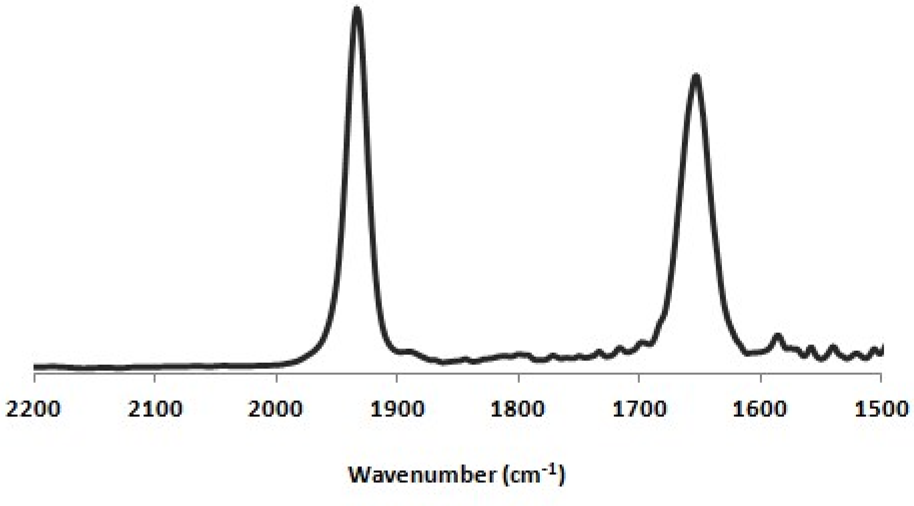

Figure S21. IR spectrum of **Co-Fe’** in CH_2Cl_2.

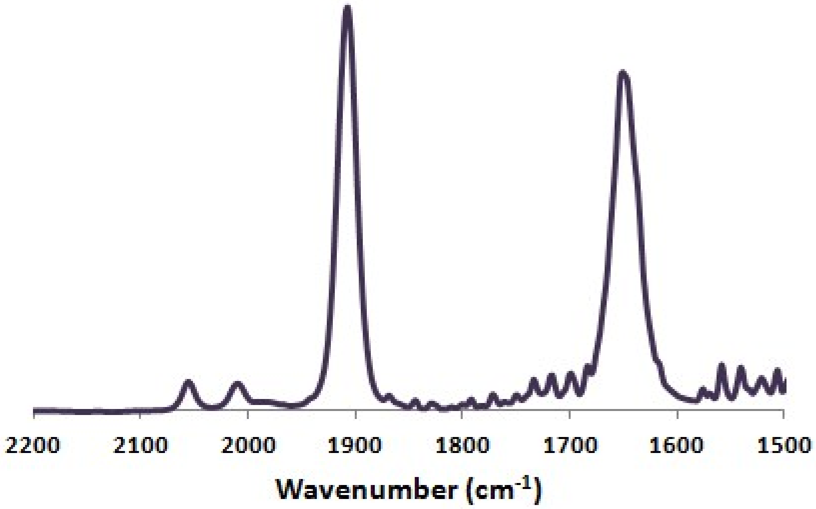

Figure S22. IR spectrum of **Co-Fe*'** in CH_2Cl_2.

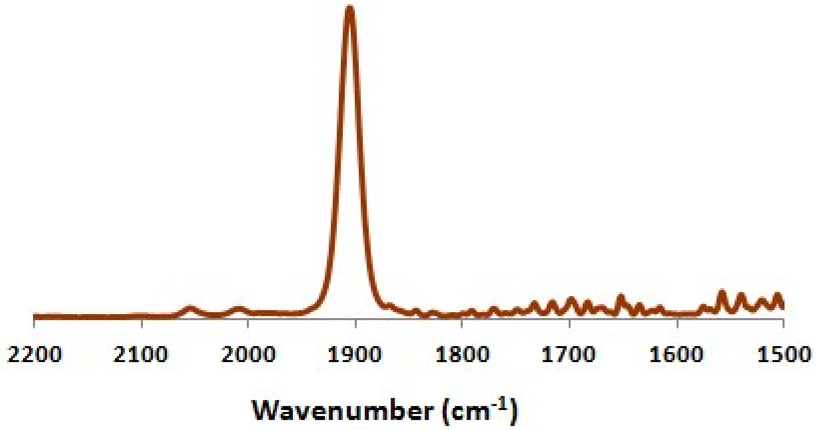

Figure S23. IR spectrum of **Ni-Fe*'** in CH_2Cl_2.

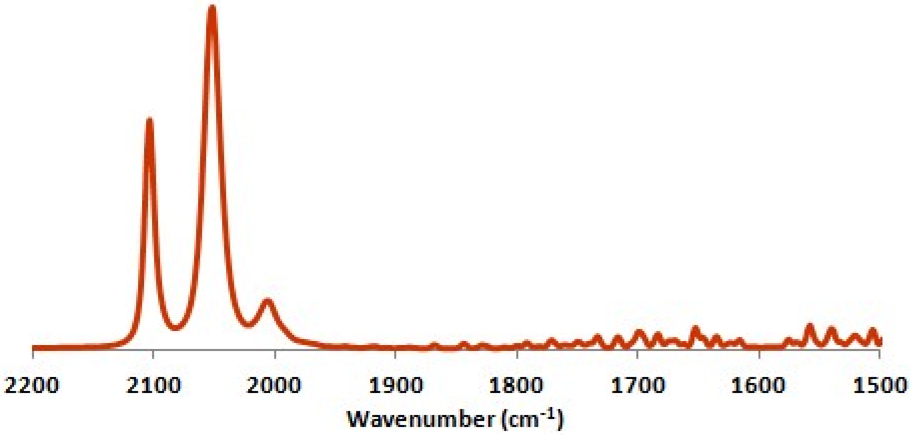

Figure S24. IR spectrum of $[(\eta^5\text{-}C_5Me_5)Fe(CO)_3]^+ [PF_6]^-$ in CH_3CN.

Positive-ion ESI Mass Spectrum:

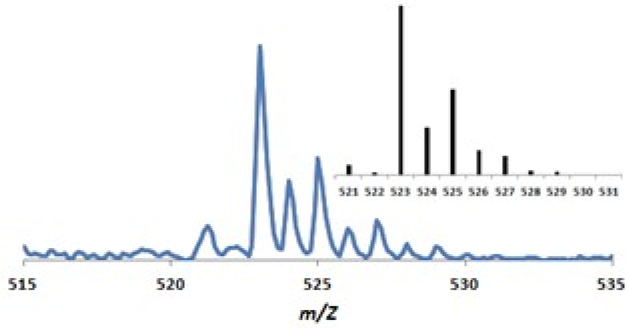

Figure S25. Positive-ion ESI mass spectrum of **Ni-Fe*" (PF_6)** in CH_3CN; inset: Calculated isotopic distribution for complex **Ni-Fe*"**.

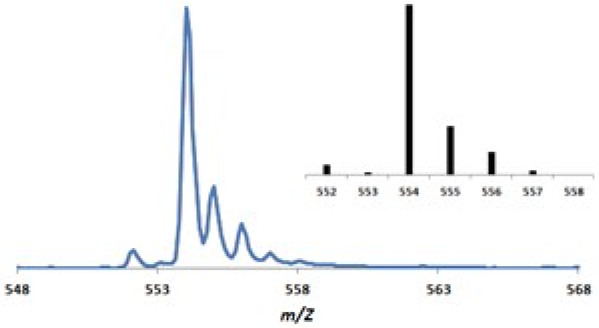

Figure S26. Positive-ion ESI mass spectrum of **Co-Fe*" (PF_6)** in CH_3CN; inset: Calculated isotopic distribution for complex **Co-Fe*"**.

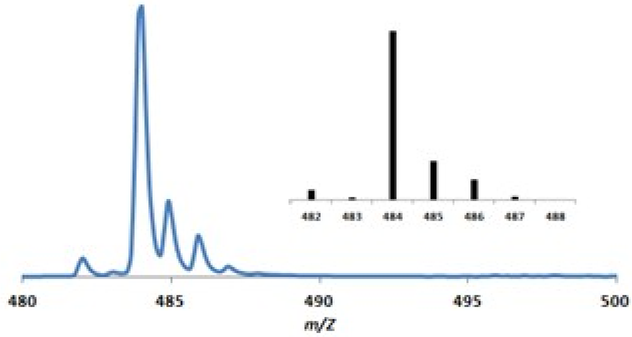

Figure S27. Positive-ion ESI mass spectrum of **Co-Fe" (BF_4)** in CH_2Cl_2; inset: Calculated isotopic distribution for complex **Co-Fe"**.

NMR Spectra:
* = residual NMR solvent

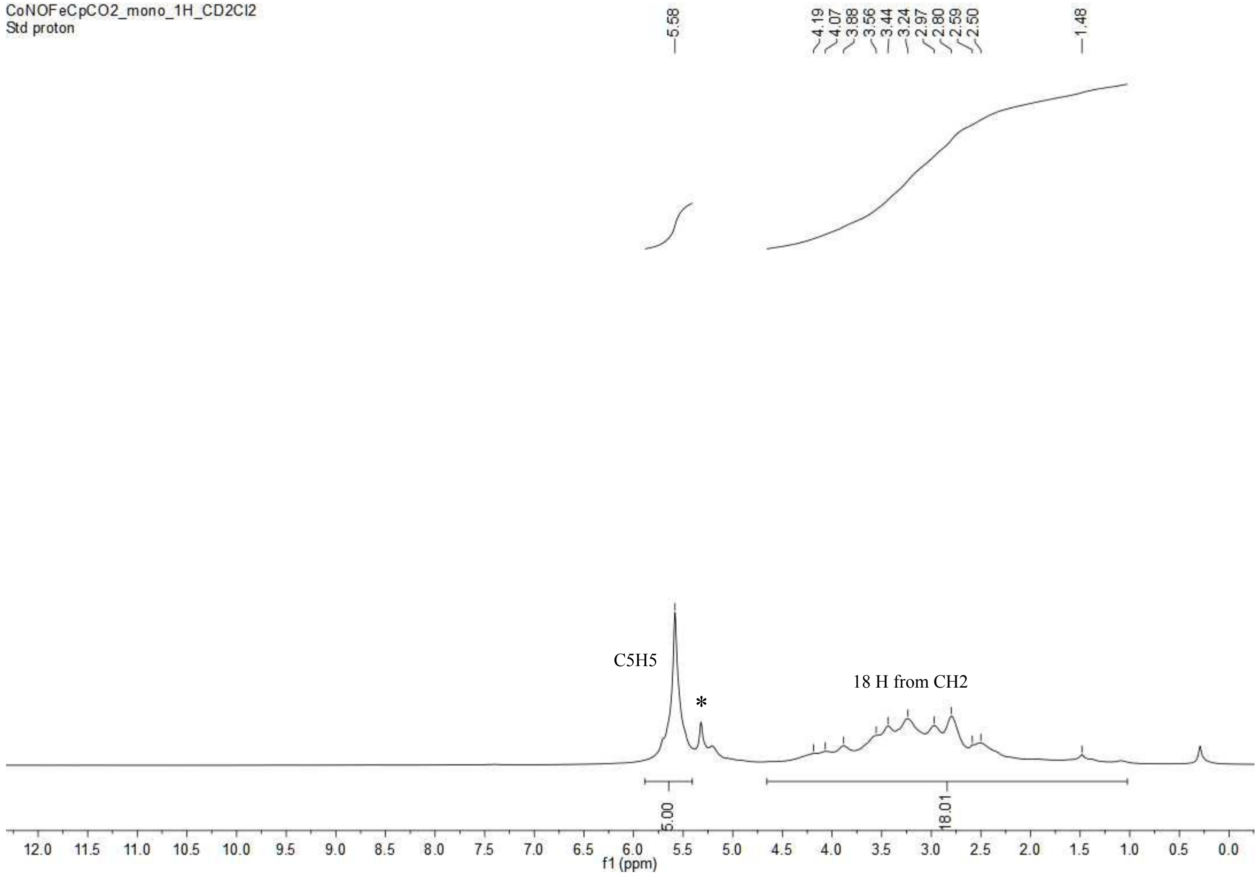

Figure S28. ^{1}H NMR Spectrum of **Co-Fe”** at 23.2 ^{o}C using a 500 MHz NMR under N_2 referenced to residual CH_2Cl_2.

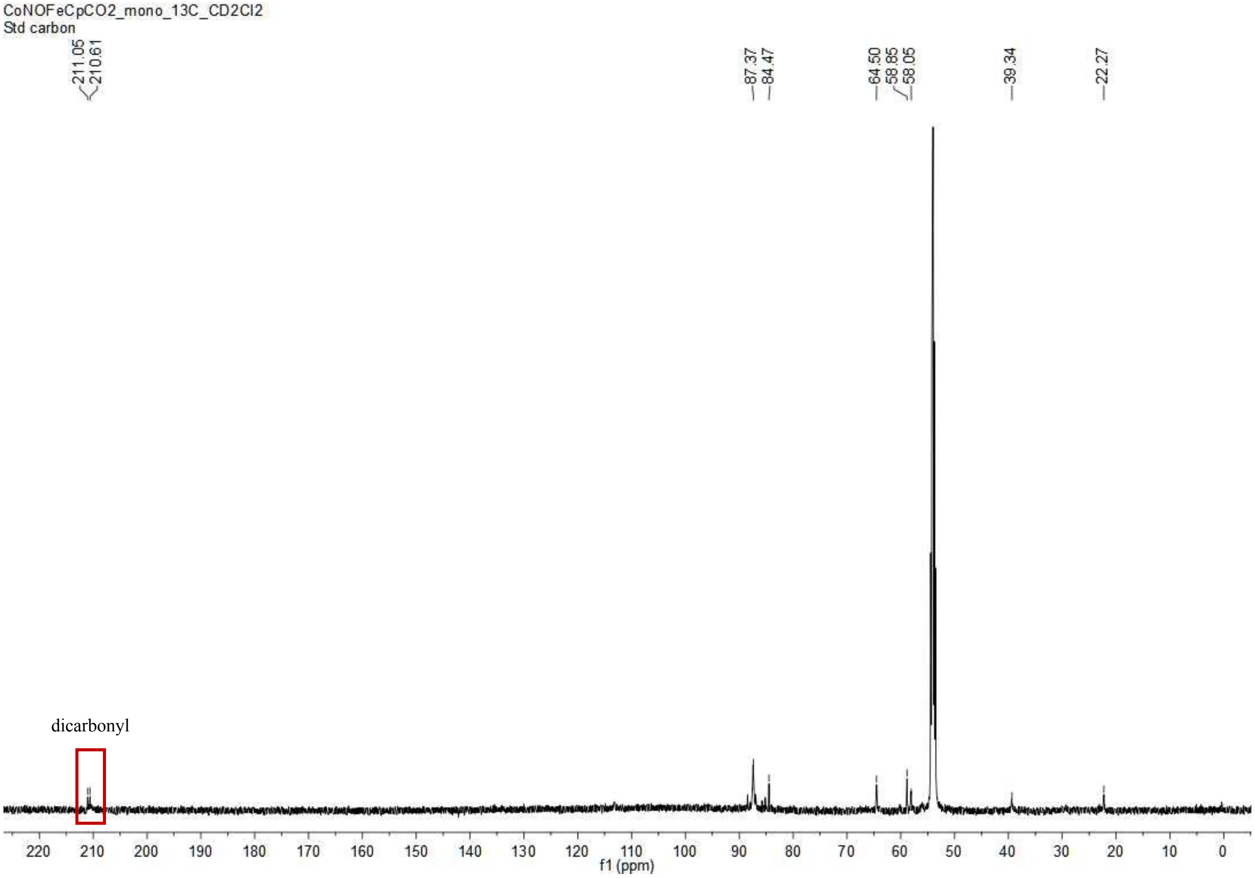

Figure S29. ^{13}C NMR Spectrum of **Co-Fe”** at 23.2 ^{o}C using a 500 MHz NMR under N_2 referenced to residual CH_2Cl_2.

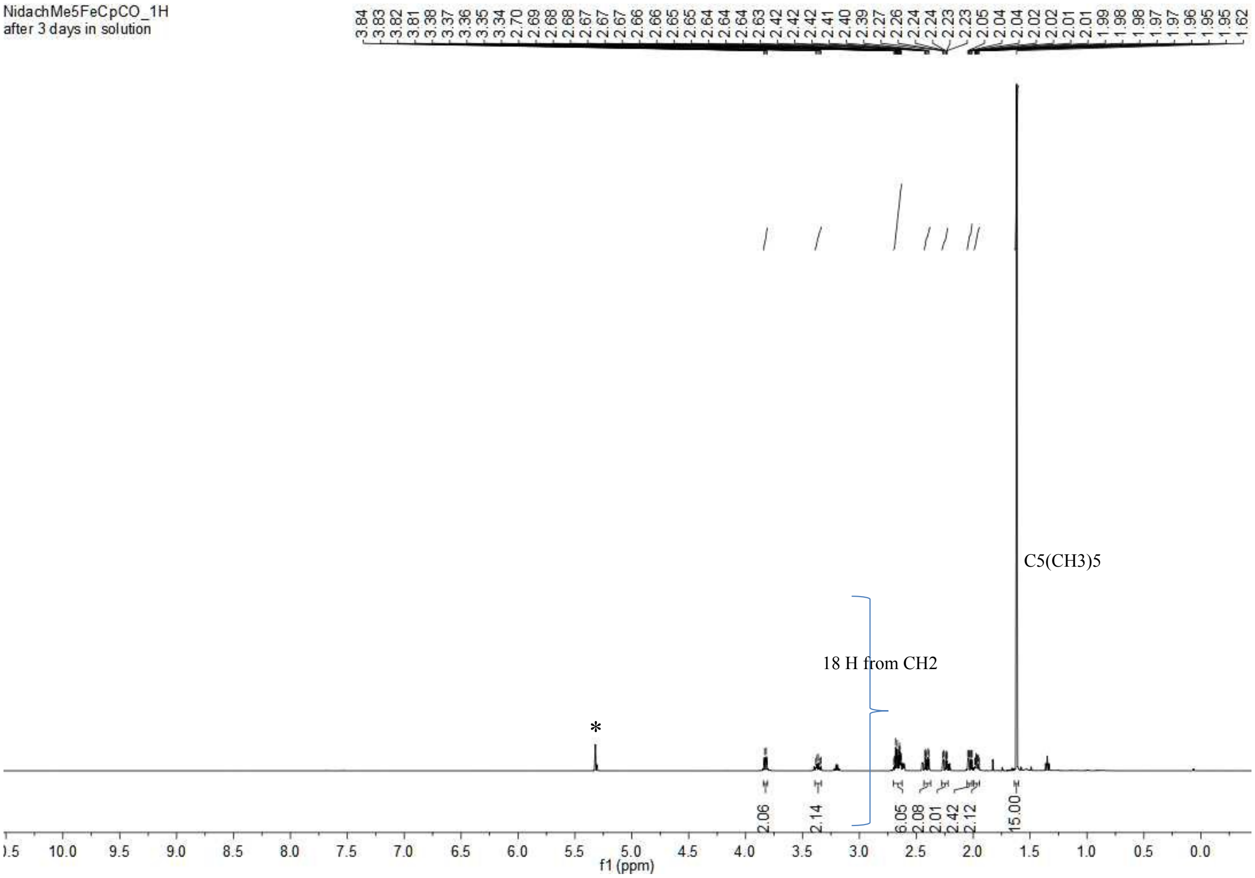

Figure S30. ^{1}H NMR Spectrum of **Ni-Fe*'** at 23.2 ^{o}C using a 500 MHz NMR under N_2 referenced to residual CH_2Cl_2.

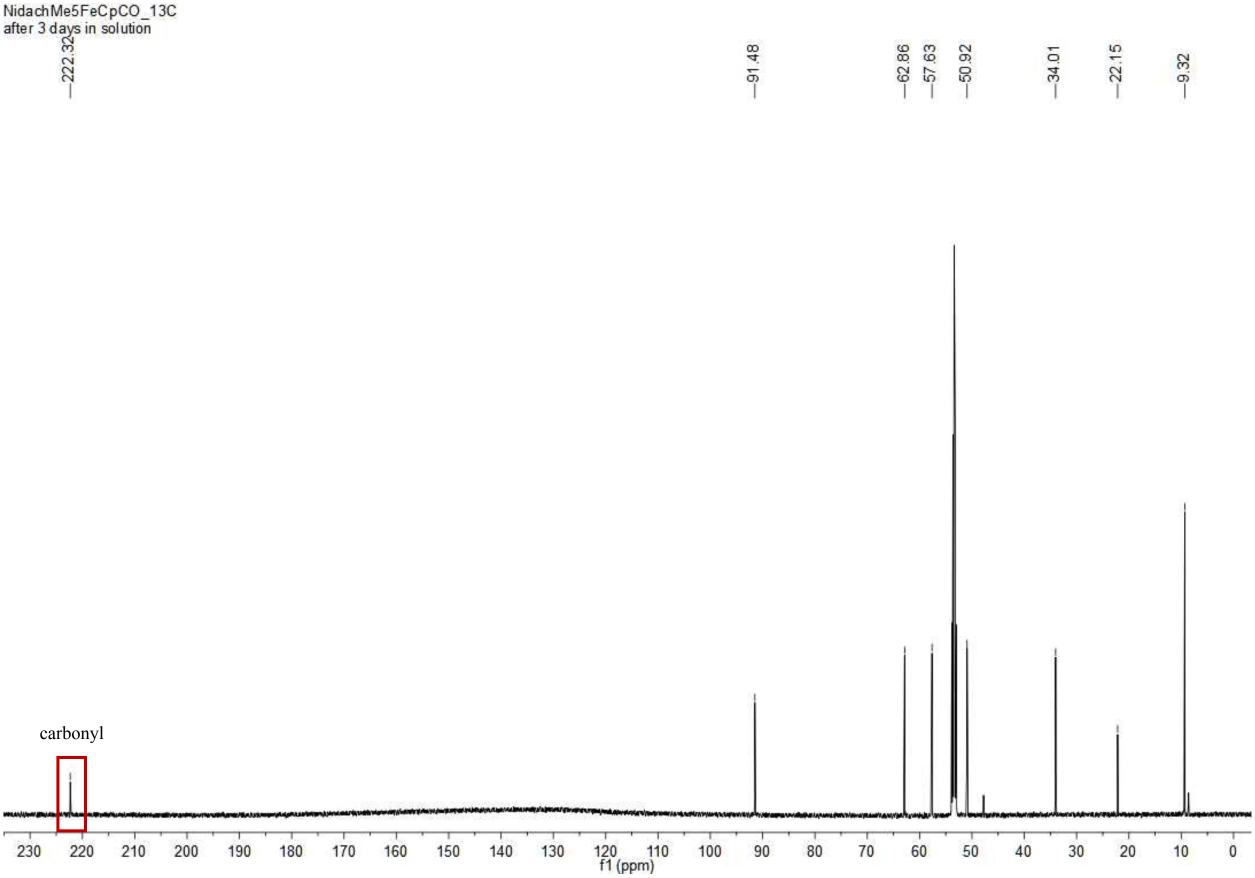

Figure S31. ^{13}C NMR Spectrum of **Ni-Fe*'** at 23.2 ^{o}C using a 500 MHz NMR under N_2 referenced to residual CH_2Cl_2.

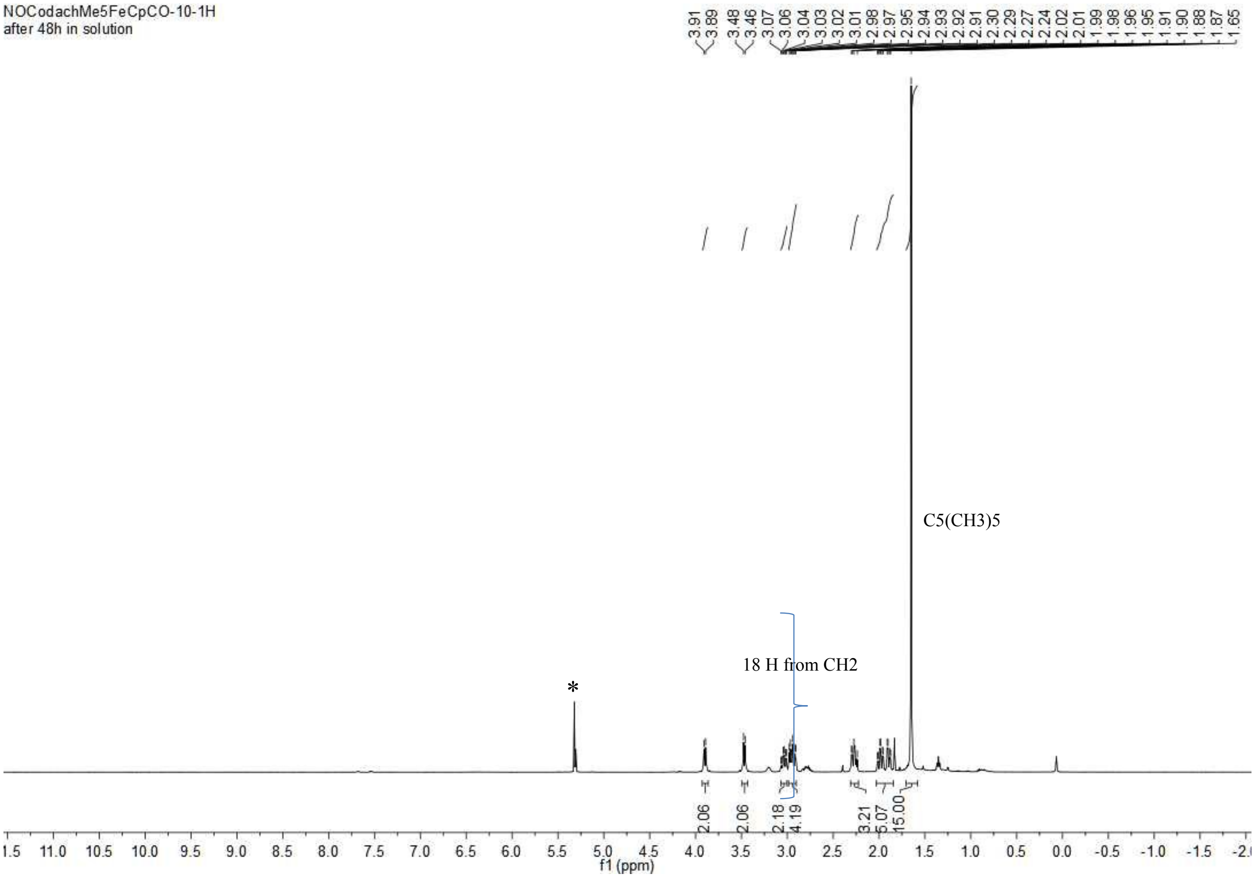

Figure S32. ^{1}H NMR Spectrum of **Co-Fe*'** at 23.2 ^{o}C using a 500 MHz NMR under N_2 referenced to residual CH_2Cl_2.

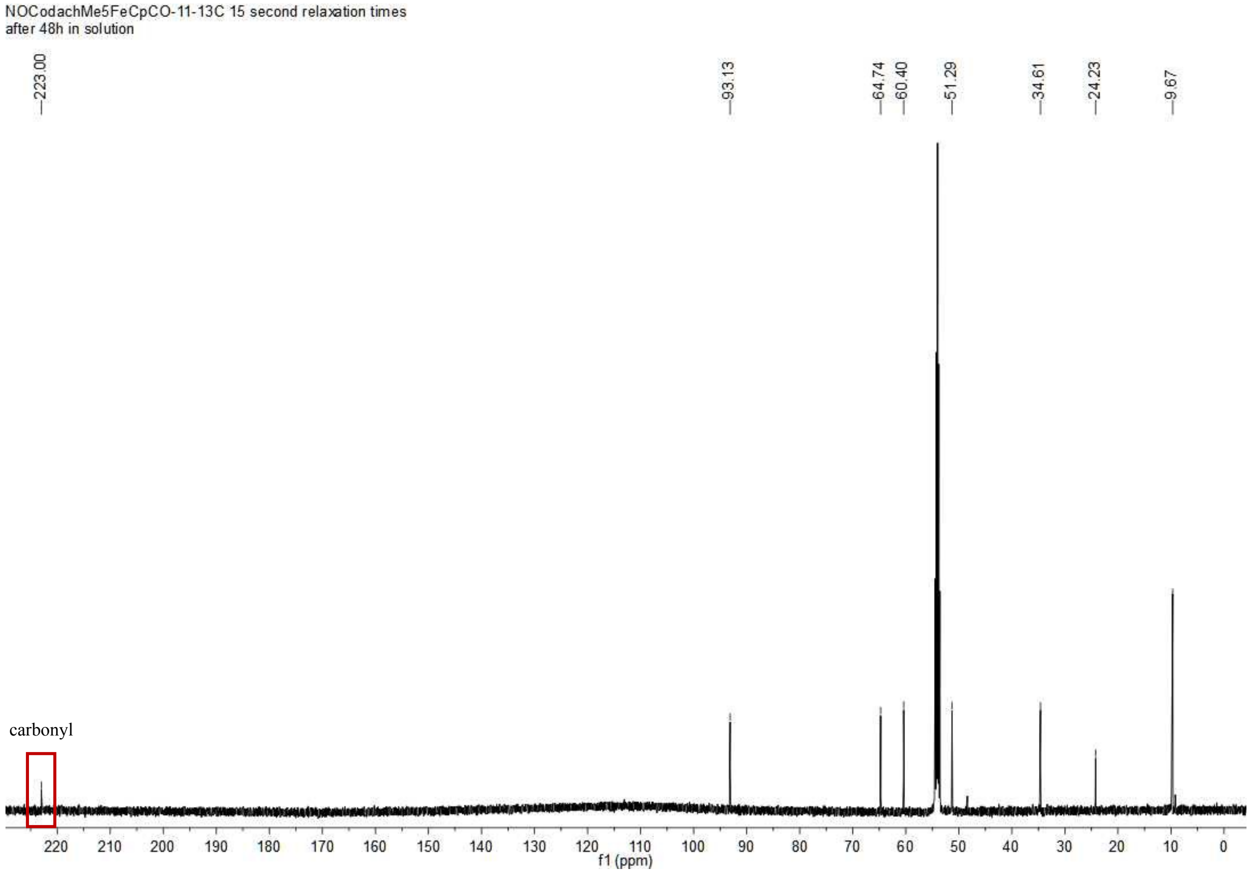

Figure S33. ^{13}C NMR Spectrum of **Co-Fe*'** at 23.2 ^{o}C using a 500 MHz NMR under N_2 referenced to residual CH_2Cl_2.

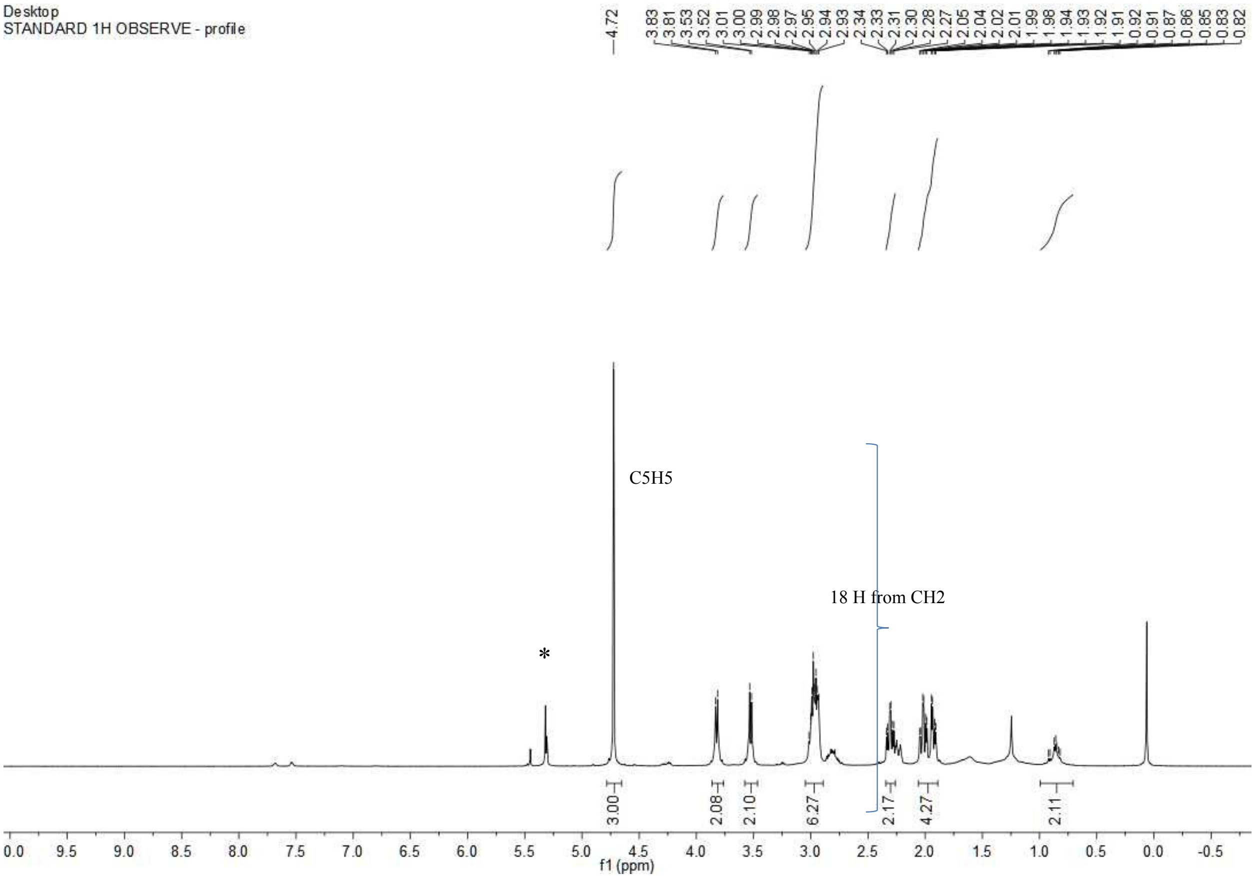

Figure S34. ^{1}H NMR Spectrum of **Co-Fe'** at 22.0 ^{o}C using a 500 MHz NMR under N_2 referenced to residual CH_2Cl_2.

Note: the integration of the 5 H's in the Cp ring does not match. This may be due to the difference in relaxation of the protons bound to the Cp ring compared to the protons on the N_2S_2 ring. The peaks between 1 and 1.75 ppm are residual grease and H_2O from NMR solvent.

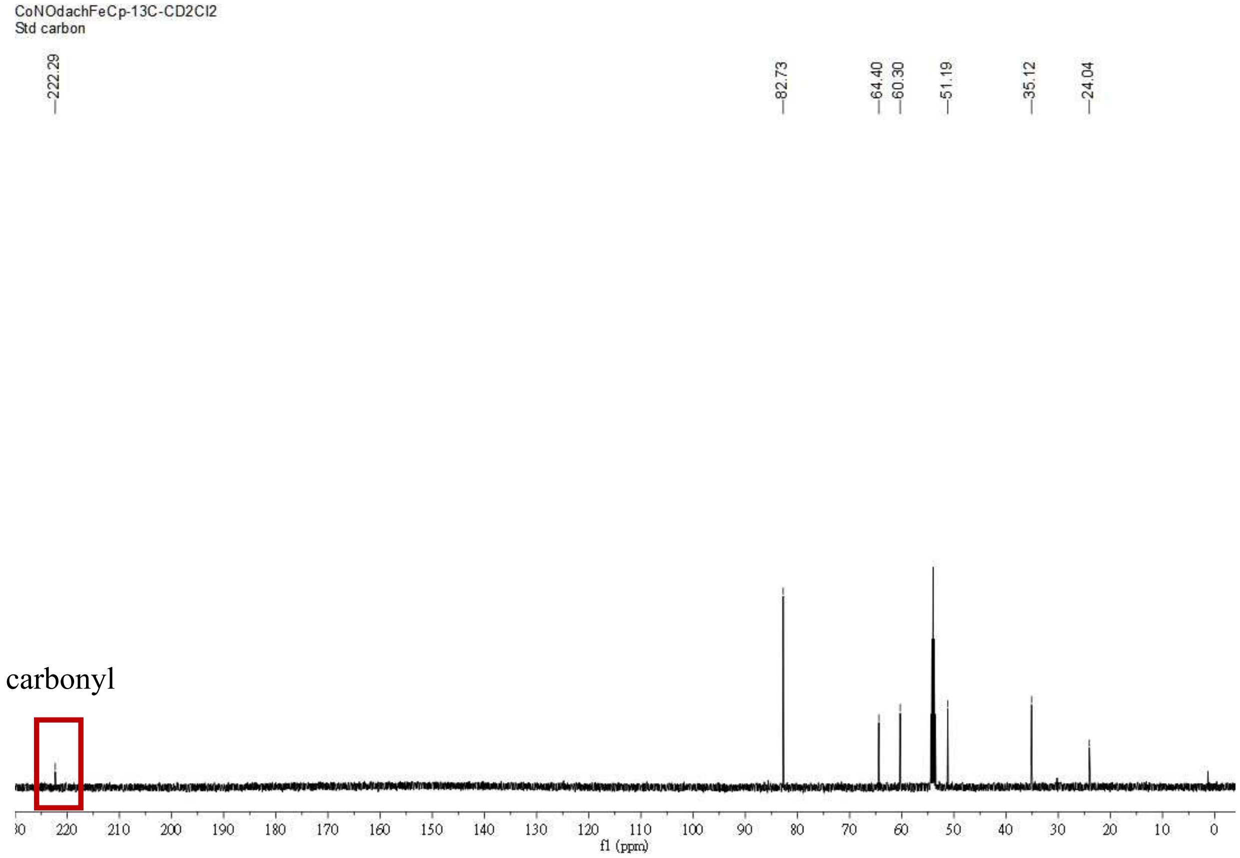

Figure S35. ^{13}C NMR Spectrum of **Co-Fe’** at 22.0 ^{o}C using a 500 MHz NMR under N_2 referenced to residual CH_2Cl_2.

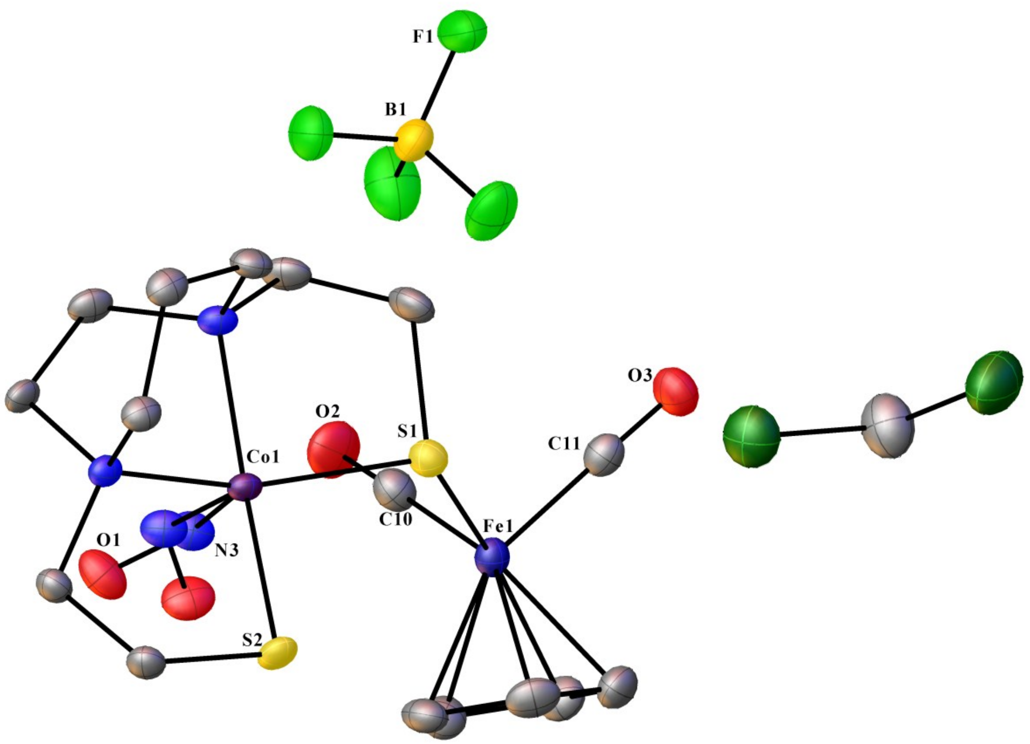

Figure S36. Thermal ellipsoid at 50 % probability for **Co-Fe”.**

Table S8. Crystal data and structure refinement for **Co-Fe”**

Identification code	cofe2co	
Empirical formula	C17 H25 B Cl2 Co F4 Fe N3 O3 S2	
Formula weight	656.01	
Temperature	150.15 K	
Wavelength	0.71073 Å	
Crystal system	Triclinic	
Space group	P-1	
Unit cell dimensions	a = 7.592(2) Å	α= 73.506(3)°.
b = 12.668(3) Å	β= 75.942(3)°.	
c = 13.662(4) Å	γ = 83.232(3)°.	
Volume	1220.5(6) Å^3	
Z	2	
Density (calculated)	1.785 Mg/m^3	
Absorption coefficient	1.721 mm^{-1}	
F(000)	664	
Crystal size	0.3 x 0.18 x 0.04 mm^3	
Theta range for data collection	1.594 to 27.530°.	
Index ranges	-9<=h<=9, -16<=k<=15, -17<=l<=17	
Reflections collected	10561	
Independent reflections	5441 [R(int) = 0.0269]	
Completeness to theta = 25.242°	99.3 %	
Absorption correction	Semi-empirical from equivalents	
Max. and min. transmission	0.7456 and 0.5325	
Refinement method	Full-matrix least-squares on F^2	
Data / restraints / parameters	5441 / 68 / 326	
Goodness-of-fit on F^2	1.040	
Final R indices [I>2sigma(I)]	R1 = 0.0348, wR2 = 0.0822	
R indices (all data)	R1 = 0.0498, wR2 = 0.0899	
Extinction coefficient	n/a	
Largest diff. peak and hole	0.637 and -0.623 e.Å^{-3}	

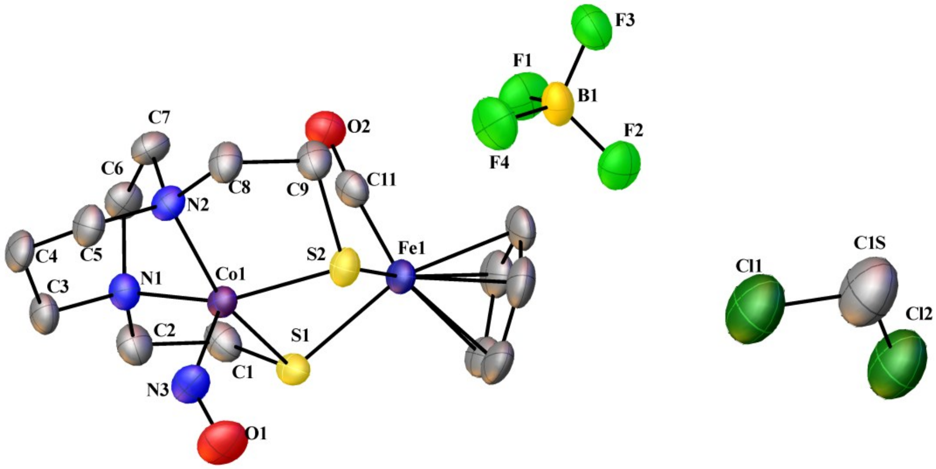

Figure S37. Thermal ellipsoid at 50 % probability for **Co-Fe'.**

Table S9. Crystal data and structure refinement for **Co-Fe'.**

Identification code	cpfeco	
Empirical formula	C15.38 H23.75 B Cl0.75 Co F4 Fe N3 O2 S2	
Formula weight	575.11	
Temperature	150.15 K	
Wavelength	0.71073 Å	
Crystal system	Orthorhombic	
Space group	F d d 2	
Unit cell dimensions	a = 24.029(4) Å	α= 90°.
b = 29.365(5) Å	β= 90°.	
c = 12.6042(17) Å	γ = 90°.	
Volume	8894(2) Å^3	
Z	16	
Density (calculated)	1.718 Mg/m^3	
Absorption coefficient	1.728 mm^{-1}	
F(000)	4669	
Crystal size	0.38 x 0.32 x 0.25 mm^3	
Theta range for data collection	1.952 to 28.405°.	
Index ranges	-32<=h<=32, -38<=k<=39, -16<=l<=16	
Reflections collected	27172	
Independent reflections	5557 [R(int) = 0.0314]	
Completeness to theta = 25.242°	99.8 %	
Absorption correction	Semi-empirical from equivalents	
Max. and min. transmission	0.7457 and 0.5961	
Refinement method	Full-matrix least-squares on F^2	
Data / restraints / parameters	5557 / 2 / 278	
Goodness-of-fit on F^2	1.065	
Final R indices [I>2sigma(I)]	R1 = 0.0344, wR2 = 0.0969	
R indices (all data)	R1 = 0.0372, wR2 = 0.0987	
Absolute structure parameter	0.019(5)	
Extinction coefficient	n/a	
Largest diff. peak and hole	1.117 and -0.531 e.Å^{-3}	

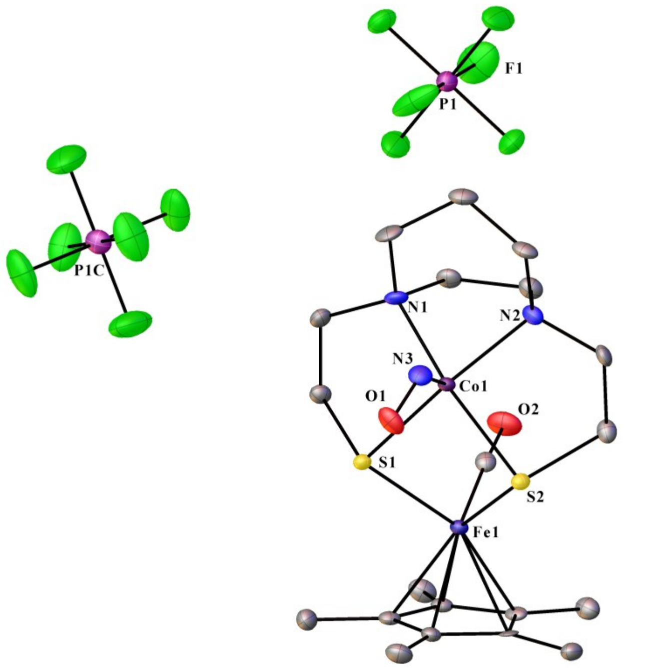

Figure S38. Thermal ellipsoid at 50 % probability for **Co-Fe*'.**

Table S10. Crystal data and structure refinement for **Co-Fe*'.**

Identification code	comcp	
Empirical formula	C20 H33 Co F6 Fe N3 O2 P S2	
Formula weight	671.36	
Temperature	110.0 K	
Wavelength	0.71073 Å	
Crystal system	Monoclinic	
Space group	C 1 2/c 1	
Unit cell dimensions	a = 22.3067(9) Å	α= 90°.
b = 21.8234(9) Å	β= 101.649(2)°.	
c = 10.8799(6) Å	γ = 90°.	
Volume	5187.3(4) Å^3	
Z	8	
Density (calculated)	1.719 Mg/m^3	
Absorption coefficient	1.489 mm^{-1}	
F(000)	2752	
Crystal size	0.125 x 0.12 x 0.082 mm^3	
Theta range for data collection	2.162 to 24.998°.	
Index ranges	-26<=h<=26, -25<=k<=25, -12<=l<=12	
Reflections collected	227516	
Independent reflections	4560 [R(int) = 0.1066]	
Completeness to theta = 24.998°	99.9 %	
Absorption correction	Semi-empirical from equivalents	
Max. and min. transmission	0.7352 and 0.6634	
Refinement method	Full-matrix least-squares on F^2	
Data / restraints / parameters	4560 / 36 / 332	
Goodness-of-fit on F^2	1.172	
Final R indices [I>2sigma(I)]	R1 = 0.0433, wR2 = 0.0756	
R indices (all data)	R1 = 0.0533, wR2 = 0.0801	
Extinction coefficient	n/a	
Largest diff. peak and hole	0.445 and -0.544 e.Å^{-3}	

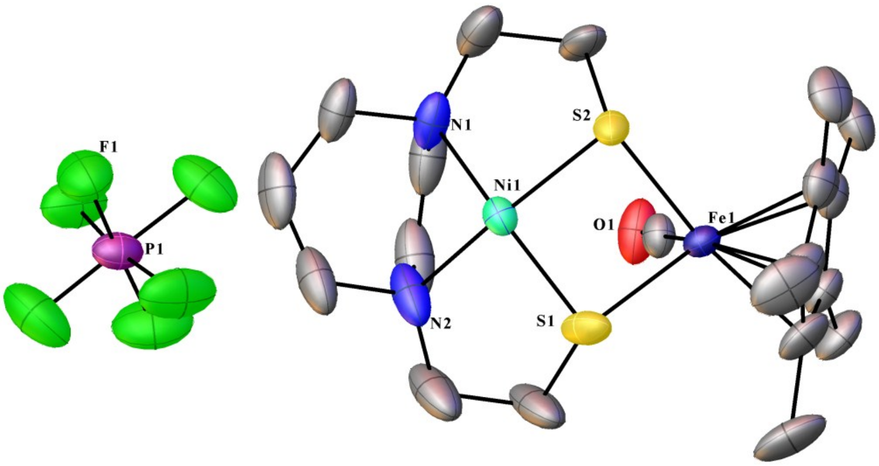

Figure S39. Thermal ellipsoid at 50 % probability for **Ni-Fe*'.**

Table S11. Crystal data and structure refinement for **Ni-Fe*'.**

Identification code	nifecpstar	
Empirical formula	C20 H33 F6 Fe N2 Ni O P S2	
Formula weight	641.13	
Temperature	100.0 K	
Wavelength	1.54178 Å	
Crystal system	Orthorhombic	
Space group	Pbca	
Unit cell dimensions	a = 12.6068(4) Å	α= 90°.
	b = 14.4727(4) Å	β= 90°.
	c = 27.5824(8) Å	γ = 90°.
Volume	5032.5(3) Å^3	
Z	8	
Density (calculated)	1.692 Mg/m^3	
Absorption coefficient	8.272 mm^{-1}	
F(000)	2640	
Crystal size	0.221 x 0.056 x 0.019 mm^3	
Theta range for data collection	3.204 to 70.215°.	
Index ranges	-15<=h<=15, -16<=k<=17, -33<=l<=33	
Reflections collected	64827	
Independent reflections	4777 [R(int) = 0.0846]	
Completeness to theta = 67.679°	99.9 %	
Absorption correction	Semi-empirical from equivalents	
Max. and min. transmission	0.7533 and 0.5155	
Refinement method	Full-matrix least-squares on F^2	
Data / restraints / parameters	4777 / 1231 / 488	
Goodness-of-fit on F^2	1.041	
Final R indices [I>2sigma(I)]	R1 = 0.0638, wR2 = 0.1507	
R indices (all data)	R1 = 0.0738, wR2 = 0.1583	
Extinction coefficient	n/a	
Largest diff. peak and hole	1.237 and -0.810 e.Å^{-3}	

References:

1. A. M. Appel and M. L. Helm, *ACS Catal.*, 2014, **4**, 630.
2. S. Wiese, U. J. Kilgore, M. –H. Ho, S. Raugei, D. L. DuBois, R. M. Bullock and M. L. Helm, *ACS Catal.*, 2013, **3**, 2527.
3. S. Ding, P. Ghosh, A. M. Lunsford, N. Wang, N. Bhuvanesh, M. B. Hall and M. Y. Darensbourg, *J. Am. Chem. Soc.*, 2016, **138**, 12920–12927.